JACS
JOURNAL OF THE AMERICAN CHEMICAL SOCIETY
Communication
pubs.acs.org/JACS

Sensitive Phonon-Based Probe for Structure Identification of 1T′ $MoTe_2$

Lin Zhou,[†,○] Shengxi Huang,[*,†,○] Yuki Tatsumi,[‡] Lijun Wu,[§] Huaihong Guo,[∥] Ya-Qing Bie,[⊥] Keiji Ueno,[#] Teng Yang,[▽] Yimei Zhu,[§] Jing Kong,[*,†] Riichiro Saito,[*,‡] and Mildred Dresselhaus[†,⊥,◆]

[†]Department of Electrical Engineering and Computer Science, Massachusetts Institute of Technology, Cambridge, Massachusetts 02139, United States

[‡]Department of Physics, Tohoku University, Sendai 980-8578, Japan

[§]Condensed Matter Physics and Materials Science Department, Brookhaven National Laboratory, Upton, New York 11973, United States

[∥]College of Sciences, Liaoning Shihua University, Fushun 113001, China

[⊥]Department of Physics, Massachusetts Institute of Technology, Cambridge, Massachusetts 02139, United States

[#]Department of Chemistry, Graduate School of Science and Engineering, Saitama University, Saitama 338-8570, Japan

[▽]Shenyang National Laboratory for Materials Science, Institute of Metal Research, Chinese Academy of Sciences, Shenyang 110016, China

Supporting Information

ABSTRACT: In this work, by combining transmission electron microscopy and polarized Raman spectroscopy for the 1T′ $MoTe_2$ flakes with different thicknesses, we found that the polarization dependence of Raman intensity is given as a function of excitation laser wavelength, phonon symmetry, and phonon frequency, but has weak dependence on the flake thickness from few-layer to multilayer. In addition, the frequency of Raman peaks and the relative Raman intensity are sensitive to flake thickness, which manifests Raman spectroscopy as an effective probe for thickness of 1T′ $MoTe_2$. Our work demonstrates that polarized Raman spectroscopy is a powerful and nondestructive method to quickly identify the crystal structure and thickness of 1T′ $MoTe_2$ simultaneously, which opens up opportunities for the in situ probe of anisotropic properties and broad applications of this novel material.

$MoTe_2$ has recently attracted enormous interests due to its novel properties[1−3] and promising applications in electronics, optoelectronics, valleytronics, spintronics, etc.[4−7] The semimetallic phases of $MoTe_2$ (1T′ and T_d) have attracted much attention and possess potential applications in quantum computing.[1−3,5] The low-temperature phase T_d $MoTe_2$, which is formed through temperature-induced phase transition from 1T′ $MoTe_2$, is a type-II Weyl semimetal, and exhibits novel quantum properties such as topological surface state Fermi arcs and chiral anomaly induced negative magnetoresistance.[2] Moreover, pressure-driven superconductivity[3] and large magnetoresistance[1] were observed in 1T′ $MoTe_2$. Besides these remarkable properties, the low-symmetry crystal structure may lead to several anisotropic properties in 1T′ $MoTe_2$. However, few works have addressed this topic because the flakes can be readily degraded in the air. To investigate the relationship between anisotropic properties and crystal structure of 1T′ $MoTe_2$, a sensitive, reliable, and nondestructive method to determine the crystal orientation is highly desirable.

Besides anisotropy, the thickness of 1T′ $MoTe_2$ also strongly affects its properties. In contrast to the semimetal bulk 1T′ $MoTe_2$, monolayer 1T′ $MoTe_2$ is predicted as large-gap quantum spin Hall insulators.[5] Since monolayer and few-layer 1T′ $MoTe_2$ easily degrade in air, measurement of the thickness using atomic force microscopy (AFM) is unpractical. Therefore, it is of great importance to develop a nondestructive, convenient method to probe the thickness of 1T′ $MoTe_2$.

In this work, we have investigated the polarization dependence of 1T′ $MoTe_2$ using polarized Raman spectroscopy with different excitation laser wavelengths. We performed transmission electron microscopy (TEM) on 1T′ $MoTe_2$ and correlate it with polarized Raman results. The combination of selected area electron diffraction (SAED), TEM, and high-angle annular dark field scanning transmission electron microscopy (HAADF-STEM) imaging and polarized Raman spectroscopy for the flakes of 1T′ $MoTe_2$ reveals the relationship between crystalline orientation and Raman intensity as a function of excitation laser wavelength, phonon symmetry, and phonon frequency. Moreover, it was found that Raman spectroscopy can also be effective in determining the thickness of 1T′ $MoTe_2$. Our work demonstrates that polarized Raman spectroscopy can be used as a powerful and nondestructive method to identify the crystal structure and thickness of 1T′ $MoTe_2$ simultaneously, which opens up opportunities for in situ probing anisotropic properties of 1T′ $MoTe_2$.

Bulk 1T′ $MoTe_2$ belongs to the space group $P2_1/m$. As illustrated in Figure 1a,b, the monoclinic structure of 1T′ $MoTe_2$ consists of a shifted Mo atom from the center of Te octahedron and the Mo atoms form the in-plane Mo−Mo bonds, resulting in zigzag Mo chains along the [010] y-direction.[8] Bulk 1T′ $MoTe_2$

Received: April 5, 2017
Published: May 25, 2017

DOI: 10.1021/jacs.7b03445
J. Am. Chem. Soc. 2017, 139, 8396−8399

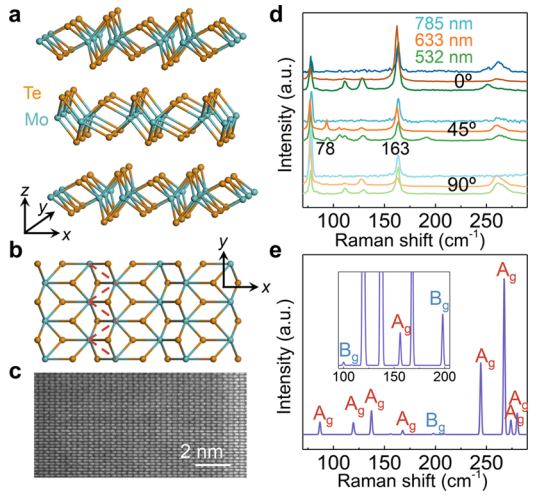

Figure 1. (a,b) Crystalline structure of the bulk 1T′ $MoTe_2$ from the perspective view (a) and top view (b). The red dashed lines in (b) denote a zigzag Mo chain. (c) HAADF-STEM image from the exfoliated 1T′ $MoTe_2$ flake. (d) Typical Raman spectra of a 1T′ $MoTe_2$ flake. (e) Calculated nonresonant Raman spectrum of bulk 1T′ $MoTe_2$.

crystal was synthesized by chemical vapor transport method. The $MoTe_2$ flakes were prepared by mechanical exfoliation onto Si/SiO_2 substrate or carbon-film TEM substrate. The HAADF-STEM image of the exfoliated 1T′ $MoTe_2$ flake (Figure 1c) confirms the monoclinic structure and high quality of the bulk 1T′ $MoTe_2$ crystal and exfoliated 1T′ $MoTe_2$ flakes.

The phonon modes of 1T′ $MoTe_2$ were investigated using polarized Raman scattering in the parallel configuration. Bulk (monolayer) 1T′ $MoTe_2$ have 36 (18) vibrational modes, and 18 (9) of them are Raman active from group theory. There is a total of 12 (6) A_g modes and 6 (3) B_g modes for bulk (monolayer) 1T′ $MoTe_2$. The calculated frequencies of the 18 (9) Raman modes are listed in Table S1(2). The typical polarized Raman spectra of a 1T′ $MoTe_2$ (5.7 nm thick) flake under different laser wavelengths (532, 633, and 785 nm) and different polarized angles (0°, 45°, and 90°) are shown in Figure 1d. In this communication, we define 0° as the [010] (y) crystal orientation, 90° as the [100] (x) orientation. The peak intensity for 1T′ $MoTe_2$ reveals strong dependence on excitation laser wavelengths and varies dramatically with polarization angles, as seen in Figure 1d. The change of the Raman spectra with different polarization angles are due to the in-plane anisotropy of 1T′ $MoTe_2$. The number of modes changes with excitation laser wavelengths and polarizations, which is relevant to resonance Raman properties and the symmetry of the wave functions, respectively, as discussed below. For the Raman spectra excited by the 532 nm laser, there are 11 Raman peaks observed at 78, 94, 104, 111, 128, 163, 190, 252, 259, 265, and 279 cm^{-1}, among which 94, 104, 111, and 190 cm^{-1} modes correspond to the B_g Raman modes and the others correspond to A_g modes (see Table S1). The Raman spectra of the 633 nm laser shows fewer peaks, and the peaks at 190, 252, and 279 cm^{-1} did not appear. Only four peaks at 78, 163, 252, and 265 cm^{-1} were observed for 785 nm laser excitation, due to the lack of resonance condition with increasing laser wavelength (Figure S3). The weakening electron−photon resonance condition from the 532 nm laser to the 785 nm laser leads to the weaker or even vanishing Raman peaks.

Moreover, the peak frequency and relative intensity also vary with excitation laser wavelengths. For example, for 0° polarization, the intensities of 163 and 78 cm^{-1} modes are similar to those for the 532 nm laser, but the intensity of 163 cm^{-1} mode becomes significantly smaller than that of 78 cm^{-1} modes for 633 and 785 nm laser. Also, it can be observed that peaks under 633 nm laser is a little red-shifted compared to other lasers. In the following, we demonstrate how Raman spectra measured under various laser excitations can be useful for the practical application of $MoTe_2$ with two major aspects: determining the crystalline orientation and flake thickness.

To probe the crystal orientation of 1T′ $MoTe_2$ and investigate how it relates to anisotropic Raman spectroscopy in 1T′ $MoTe_2$, SAED, TEM, HAADF-STEM, and polarized Raman spectroscopy were performed on the same 1T′ $MoTe_2$ flakes with various thickness. Figure 2a presents a typical optical microscope image of

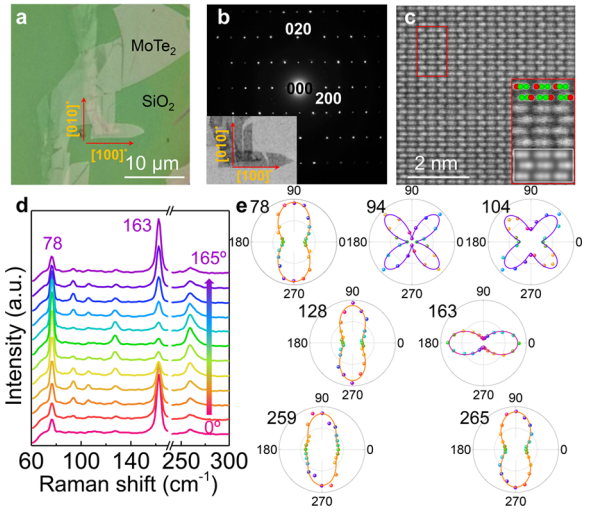

Figure 2. (a) Optical microscope image of exfoliated 1T′ MoTe2 flakes on TEM grid. The arrows labeled by [100]* and [010]* (superscript * indicates the index in reciprocal space) are determined from SAED pattern in (b). (b) SAED pattern from the area shown in (a). The TEM image is shown in the inset. (c) High-resolution HAADF-STEM image from the 1T′ $MoTe_2$ flake. The inset with red frame is the magnified image from the red rectangle area. [001] atomic projection of the 1T′ is embedded with red and green spheres representing Mo and Te atoms, respectively. The white framed inset shows the simulated image based on 1T′ crystal structure, which is consistent with the experimental image. (d) Polarized Raman spectra (633 nm laser excitation) of the same 1T′ $MoTe_2$ flake measured with polarization angle from 0° (bottom) to 165° (top) with an interval of 15°. (e) Polar plots of Raman intensity as a function of polarization angles for different Raman modes.

1T′ $MoTe_2$ flakes protected by TEM grid and PMMA layer. The corresponding SAED pattern of the 1T′ $MoTe_2$ flake shows rectangular pattern (Figure 2b), which can be indexed with the monoclinic structure of the 1T′ phase, and used to determine the crystal orientation on this specific flake. The corresponding HAADF-STEM image in Figure 2c matches well with the image simulation based on the 1T′ $MoTe_2$ structure, shown in the inset of Figure 2c, which unambiguously points out the crystal orientation of the flake and verifies the high-quality of exfoliated flakes.

We measured the polarized Raman spectra and corresponding crystal orientation by TEM on 1T′ $MoTe_2$ flake, presented in Figure 2d. It can be observed clearly that the peak intensities change with polarization angles in different ways. Seven Raman modes are observed, among which five are of A_g symmetry (78, 128, 161, 259, and 265 cm^{-1}) and two are of B_g symmetry (94 and 104 cm^{-1}) (Figure 2d). As shown in Figure 2e, the Raman polar

DOI: 10.1021/jacs.7b03445
J. Am. Chem. Soc. 2017, 139, 8396−8399

plots correspond well to the crystalline orientation determined by TEM. The intensities of the four A_g Raman peaks at 78, 128, 259, and 265 cm^{-1} vary with a period of 180°, and the maximum intensities appear at a specific polarization angle along with the [100] crystal axis. In contrast, for the A_g Raman peak around 161 cm^{-1}, the maximum intensity occurs when the polarization angle is along with the [010] crystal axis. We also noticed that for some modes, such as 259 cm^{-1} mode, the minimum Raman intensity is not along 0° since there is a small secondary maximum near 0°. This phenomenon, also observed in other layered materials with in-plane anisotropy,[9−12] originates from the optical absorption that induces phase mismatch for the Raman tensor elements along different crystal orientations. For the two B_g Raman peaks at 94 and 104 cm^{-1}, the intensities change in a period of 90°, with maximum intensities at 45° and minimum at 0° and 90°. For each mode, such relationship between crystal orientation and Raman intensity remains the same for flakes with different thicknesses. Thus, the combined TEM/Raman measurements unambiguously reveal the relationship between Raman signals and crystal orientation. More importantly, this nondestructive, sensitive, and fast anisotropic Raman characterization provides a reliable method to obtain the crystal information on 1T′ $MoTe_2$ with various thicknesses.

The Raman anisotropy of 1T′ $MoTe_2$ flake has remarkable changes under different excitation laser wavelengths. Polarized Raman using three excitation laser wavelengths (532, 633, and 785 nm) were measured on 1T′ $MoTe_2$ flakes with various thicknesses on Si/SiO_2 substrates. The flakes that are physically connected were selected to ensure the same crystalline orientation. The Raman polar plots of a typical flake are summarized in Table 1. Raman polar plots for other flakes are presented in Tables S3 and S4. We have noticed several observations from the tables.

Table 1. Raman Polar Plots of a Typical Flake (5.7 nm thick) of Various Raman Modes under Different Incident Laser

mode (cm^{-1})	532 nm	633 nm	785 nm	mode (cm^{-1})	532 nm	633 nm	785 nm
78				190			
94				252			
104				259			
111				265			
128				279			
163							

Raman modes, even with the same symmetry, can show different anisotropy under the same laser excitation wavelengths. For example, for the A_g modes under 532 nm laser, 78, 111, 128, 163, and 252 cm^{-1} modes show that maximum intensities are along 0° (violet fitted curve in Table 1), while 259, 265, and 279 cm^{-1} modes have their maximum intensities along 90° (orange fitted curve in Table 1).

For the same Raman mode, the Raman anisotropy can change their orientations with changing laser wavelengths. For example, 78 cm^{-1} mode shows the maximum intensity along 0° under 532 nm laser, but along 90° under 633 and 785 nm laser; 128 cm^{-1} mode shows the maximum intensity along 0° under 532 nm laser, but along 90° under 633 nm laser. Some modes change degree of anisotropy with laser wavelengths, and some even become isotropic under certain laser excitations. For example, 163 cm^{-1} shows stronger anisotropy under 633 nm laser than under 532 nm laser, and under 785 nm laser, it shows isotropic Raman intensity. This phenomenon can be attributed to the optical transition selection rule, which is discussed in detail in the Supporting Information (SI). In short, by changing the laser excitation energies, the final or initial electronic states with the different symmetry of the wave functions are selected so as to satisfy the resonance condition. Then the electron−photon matrix elements can have unique polarization dependence even for the same phonon modes that satisfies the group theory. For flakes with different thicknesses from few-layer to bulk, Raman anisotropy orientations do not change for each mode (Tables 1, S3, and S4). This feature can tremendously simplify the method of using polarized Raman to determine crystalline orientation since the flake thickness does not need to be taken into consideration.

Overall, it can be seen that polarized Raman is a sensitive probe to determine the crystalline orientation of 1T′ $MoTe_2$, but some cautions need to be taken on the selection of excitation laser wavelength due to the sensitivity of Raman anisotropy with laser wavelength.

The frequencies of 78 and 259 cm^{-1} modes exhibit a monotonic redshift when the thickness is increased (Figure 3a). As shown in Figure 3c, for the few-layer flake (thickness 3.7 nm), the 78 cm^{-1} mode under 633 nm has the frequency of nearly 80 cm^{-1}, but as the thickness increases to 33.5 nm, its frequency decreases to ∼77.7 cm^{-1}. Similar trends were also observed for 532 and 785 nm lasers (Figure 3b,d). For the 259 cm^{-1} mode with 633 nm laser, the frequency decrease from 262.4 to 259.2 cm^{-1} for thickness increases from 5.2 to 33.5 nm (Figure 3e). The frequencies measured here are chosen for the polarization with the maximum intensity (or minimum intensity) of the modes to minimize the uncertainty of the measured frequency. One possible reason for such a frequency drop with increased thickness is the increase of dielectric screening of the long-range Coulomb interaction for an excitation going from few-layer to multilayer $MoTe_2$.[13] In particular, the 78 cm^{-1} mode remains high intensity under variable polarization angles, and the frequency is insensitive to polarization. Thus, the 78 cm^{-1} mode is a good identification for thickness, even for arbitrary polarization angle.

Another method to determine the thickness of flakes is the intensity ratio of 259 to 252 cm^{-1} modes. As shown in Figure 3f, the ratio is 0.7 for the flake thickness of 3.2 nm, but increases monotonically to 3.5 for the 33.5 nm thick flake. The mechanism that $I(259)/I(252)$ increases with layer thickness is possibly the opposite trend of $I(259)$ measured by x-polarized light and $I(252)$ measured by y-polarized light changing with thickness (see details in SI).

In conclusion, we have demonstrated Raman spectroscopy as a nondestructive and convenient way to determine the crystalline orientation and flake thickness of 1T′ $MoTe_2$. We also perform TEM analysis on 1T′ $MoTe_2$ and successfully correlate it with polarized Raman. We found that the polarized Raman can be effectively used to determine the crystalline orientation of 1T′ $MoTe_2$ flake with thicknesses ranging from few-layer to bulk. Due to the sensitivity of Raman anisotropy with laser excitation wavelengths, special attentions should be paid on the laser wavelength used when determining the crystalline orientation. In

DOI: 10.1021/jacs.7b03445
J. Am. Chem. Soc. 2017, 139, 8396−8399

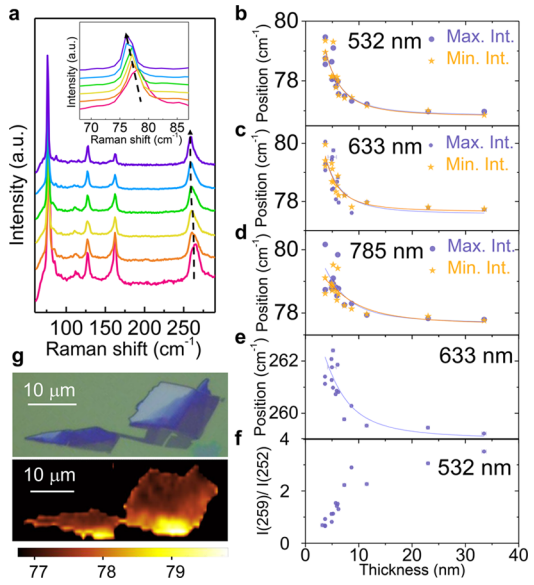

Figure 3. (a) Raman spectra of 1T′ $MoTe_2$ flakes with different thicknesses. Thickness from bottom to top: 3.6, 5.1, 5.8, 6.3, 8.5, and 31 nm. The inset shows the zoom-in of 78 cm^{-1} peak. The spectra were measured under 633 nm laser and along 90° crystal orientation. The spectra intensities are normalized by the corresponding 78 cm^{-1} mode. (b–d) The frequency change of 78 cm^{-1} mode with flake thickness under 532, 633, and 785 nm laser, respectively. (e) The frequency change of 259 cm^{-1} mode with flake thickness measured under 633 nm laser. (f) The thickness dependence of intensity ratio of 259 and 252 cm^{-1} modes measured under 532 nm laser. Both intensities of (e) and (f) are selected with the polarization for their corresponding maximum intensities, i.e., 90° for 259 cm^{-1} mode and 0° for the 252 cm^{-1} mode. (g) Optical image of the flakes (top) and Raman mapping of the 78 cm^{-1} mode frequency (bottom). Despite the insensitivity of Raman anisotropy to flake thickness, several Raman features, including peak frequency and intensity ratio, varies with the thickness of 1T′ $MoTe_2$ flakes. We found that the A_g modes at 78 and 259 cm^{-1} as well as the intensity ratio $(I(259)/I(252))$ can be used for the identification of the thickness of 1T′ $MoTe_2$ sample.

addition, the thickness of the flakes can be determined using two ways: the frequency of 78 and 259 cm^{-1} modes and the intensity ratio of 259 and 252 cm^{-1} modes. The former decreases and the latter increases with increased thickness of the flakes. These experimental observations can be well explained using group theory and DFT calculations. Our work provides insights into the phonon property of the anisotropic material and paves the way for broad applications of 1T′ $MoTe_2$.

■ ASSOCIATED CONTENT

Supporting Information

The Supporting Information is available free of charge on the ACS Publications website at DOI: 10.1021/jacs.7b03445.

Experimental details and supplementary figures (PDF)

■ AUTHOR INFORMATION

Corresponding Authors

*jingkong@mit.edu
*rsaito@flex.phys.tohoku.ac.jp
*shengxih@mit.edu

ORCID

Huaihong Guo: 0000-0001-7094-2878
Jing Kong: 0000-0003-0551-1208

Author Contributions

○These authors contribute equally to this work.

Notes

The authors declare no competing financial interest.
◆Deceased author.

■ ACKNOWLEDGMENTS

We acknowledge financial support by STC Center for Integrated Quantum Materials, NSF Grant No. DMR-1231319, EFRI 2-DARE(EFMA-1542815), NSF grant DMR-1507806, and the U.S. Army Research Office through the MIT Institute for Soldier Nanotechnologies (Grant No. 023674). Work on Raman measurement by L.Z., S.H., and M.D. was supported by the Solid-State Solar-Thermal Energy Conversion Center (S3TEC), an Energy Frontier Research Center funded by DOE, Office of Science, BES under Award #DE-SC0001299/DE-FG02-09ER46577. We acknowledge Ms. Baojuan Dong for the help with the nonresonant Raman spectra calculations. T.Y. acknowledges the NSFC under Grants 1331006 and U1537204 for financial support. R.S. and K.U. acknowledge JSPS KAKENHI Grant Numbers JP25286005, JP25107005, and JP15K21722. L.W. and Y.Z. acknowledge the U.S. Department of Energy, Office of Basic Energy Science, Division of Materials Science and Engineering, under Contract No. DE-SC0012704.

■ REFERENCES

(1) Keum, D. H.; Cho, S.; Kim, J. H.; Choe, D.-H.; Sung, H.-J.; Kan, M.; Kang, H.; Hwang, J.-Y.; Kim, S. W.; Yang, H.; Chang, K. J.; Lee, Y. H. *Nat. Phys.* **2015**, *11*, 482.

(2) Deng, K.; Wan, G.; Deng, P.; Zhang, K.; Ding, S.; Wang, E.; Yan, M.; Huang, H.; Zhang, H.; Xu, Z.; Denlinger, J.; Fedorov, A.; Yang, H.; Duan, W.; Yao, H.; Wu, Y.; Fan, S.; Zhang, H.; Chen, X.; Zhou, S. *Nat. Phys.* **2016**, *12*, 1105.

(3) Qi, Y.; Naumov, P. G.; Ali, M. N.; Rajamathi, C. R.; Schnelle, W.; Barkalov, O.; Hanfland, M.; Wu, S.-C.; Shekhar, C.; Sun, Y.; Susz, V.; Schmidt, M.; Schwarz, U.; Pippel, E.; Werner, P.; Hillebrand, R.; Forster, T.; Kampert, E.; Parkin, S.; Cava, R. J.; Felser, C.; Yan, B.; Medvedev, S. A. *Nat. Commun.* **2016**, *7*, 11038.

(4) Cho, S.; Kim, S.; Kim, J. H.; Zhao, J.; Seok, J.; Keum, D. H.; Baik, J.; Choe, D.-H.; Chang, K. J.; Suenaga, K.; Kim, S. W.; Lee, Y. H.; Yang, H. *Science* **2015**, *349*, 625.

(5) Qian, X.; Liu, J.; Fu, L.; Li, J. *Science* **2014**, *346*, 1344.

(6) Zhang, Q.; Yang, S. A.; Mi, W.; Cheng, Y.; Schwingenschlögl, U. *Adv. Mater.* **2016**, *28*, 959.

(7) Zhou, L.; Xu, K.; Zubair, A.; Liao, A. D.; Fang, W.; Ouyang, F.; Lee, Y.-H.; Ueno, K.; Saito, R.; Palacios, T.; Kong, J.; Dresselhaus, M. S. *J. Am. Chem. Soc.* **2015**, *137*, 11892.

(8) Brown, B. *Acta Crystallogr.* **1966**, *20*, 268.

(9) Beams, R.; Cançado, L. G.; Krylyuk, S.; Kalish, I.; Kalanyan, B.; Singh, A. K.; Choudhary, K.; Bruma, A.; Vora, P. M.; Tavazza, F.; Davydov, A. V.; Stranick, S. J. *ACS Nano* **2016**, *10*, 9626.

(10) Ribeiro, H. B.; Pimenta, M. A.; de Matos, C. J. S.; Moreira, R. L.; Rodin, A. S.; Zapata, J. D.; de Souza, E. A. T.; Castro Neto, A. H. *ACS Nano* **2015**, *9*, 4270.

(11) Ling, X.; Huang, S.; Hasdeo, E. H.; Liang, L.; Parkin, W. M.; Tatsumi, Y.; Nugraha, A. R. T.; Puretzky, A. A.; Das, P. M.; Sumpter, B. G.; Geohegan, D. B.; Kong, J.; Saito, R.; Drndic, M.; Meunier, V.; Dresselhaus, M. S. *Nano Lett.* **2016**, *16*, 2260.

(12) Huang, S.; Tatsumi, Y.; Ling, X.; Guo, H.; Wang, Z.; Watson, G.; Puretzky, A. A.; Geohegan, D. B.; Kong, J.; Li, J.; Yang, T.; Saito, R.; Dresselhaus, M. S. *ACS Nano* **2016**, *10*, 8964.

(13) Shim, G. W.; Yoo, K.; Seo, S.-B.; Shin, J.; Jung, D. Y.; Kang, I.-S.; Ahn, C. W.; Cho, B. J.; Choi, S.-Y. *ACS Nano* **2014**, *8*, 6655.

DOI: 10.1021/jacs.7b03445
J. Am. Chem. Soc. 2017, 139, 8396–8399